Student Conference Proceedings
Vol 2, No 1, 2026, Article ID 2583, 4 Pages

Student Conference Lübeck

Proceedings Article

Iterative image deconvolution for resolution enhancement in X-ray non-destructive testing

Julian Althaus[a,b,*] · Kevin Eickhoff[b] · Frank Herold[b] · Maik Stille[c,*]

[a] Study program Medical Engineering Science, Universität zu Lübeck, Lübeck, Germany
[b] VisiConsult X-ray Systems & Solutions GmbH, Stockelsdorf, Germany
[c] Fraunhofer Research Institute for Individualized Medical Technology and Engineering IMTE, Lübeck, Germany
[*] Corresponding author, email: julian.althaus@student.uni-luebeck.de; maik.stille@imte.fraunhofer.de

Received 27 April 2026; Accepted 14 October 2026; Published online 27 October 2026

© 2026 Julian Althaus *et al.*; licensee Infinite Science Publishing
This is an Open Access article distributed under the terms of the Creative Commons Attribution License (http://creativecommons.org/licenses/by/4.0), which permits unrestricted use, distribution, and reproduction in any medium, provided the original work is properly cited.

Abstract

X-ray is a widely used technique in industrial and medical imaging. Especially for non-destructive testing of safety-critical components, high spatial resolution is crucial for the reliable detection of subtle details. To this end, iterative image deconvolution is a common approach in photography and microscopy to retrospectively improve spatial resolution. In this work, the iterative Richardson-Lucy (RL) deconvolution algorithm is applied to X-ray images for various models of the point spread function (PSF), based on the slanted edge method. The image quality is evaluated using the interpolated basic spatial resolution (iSR_b) based on the ASTM E2002 standard, allowing for RL parameter optimization. Using optimized damping and iteration parameters, a resolution improvement of over nine percent with limited artifact formation is achieved. The results show that RL deconvolution is a promising approach for improving spatial resolution, offering high potential for industrial X-ray.

I. Introduction

Obtaining high-resolution X-ray images remains challenging due to limitations of current detection methods [1], [2]. However, high resolution is essential for non-destructive testing to detect defects with high precision in safety-critical components, e.g. in aerospace [3]. In radiography, the limited number of detected photons plays a particularly important role in image quality. Here, the use of thicker scintillators increases the number of detected photons and thus improves the signal-to-noise ratio. However, thicker scintillators increase energy-dependent blurring due to optical diffusion within the detector, broadening the point spread function (PSF) of the detection system and degrading image quality [1], [2]. On the one hand, this issue can be tackled by either very costly high-precision hardware (e.g. needle-structured scintillators), which are not feasible for all applications, or by thinner scintillators at the expense of longer exposure times [4]. On the other hand, image quality can be improved retrospectively by image deconvolution as a post-processing step. In this approach, the measured image I is expressed as a convolution ($*$) of the latent sharp image I_S with the PSF and additional noise θ (i.e. $I = I_S * \mathrm{PSF} + \theta$). Consequently, accurate estimates of the PSF and noise are crucial to avoid artifacts after deconvolution [4]. The Richardson-Lucy (RL) algorithm [5], [6], a popular iterative deconvolution algorithm in photography and microscopy, offers a useful approach for this challenge [4], [7]. Compared to the widely used Wiener filter, RL provides an iterative framework in which ringing artifacts can be effectively controlled using a damping parameter. However, RL remains sensitive to noise and requires parameter tuning, complicating its application to industrial X-ray imaging [4], [7]. This study addresses these challenges by first identifying an accurate estimate of the detector-specific PSF for the RL deconvolution. Subsequently, the rele-

© 2026 Infinite Science Publishing

vant RL parameters are systematically studied and optimized to achieve improved image quality.

II. Methods and material

This section describes the estimation of the PSF for iterative image deconvolution and introduces a metric to assess the achieved resolution enhancement in X-ray nondestructive testing.

II.I. Extracting the PSF

In this work, the PSF is directly estimated from image space. For this purpose, the intensity profile perpendicular to a slanted edge is measured to obtain the edge spread function (ESF), representing the intensity distribution after optical system processing (cf. Fig. 1(b)). To obtain a more reliable result, ten ESFs were extracted and averaged (see red lines in Fig. 1(a)). The line spread function (LSF) is defined as the derivative of the ESF ($\mathrm{LSF}(x) = d_x \mathrm{ESF}(x)$, see Fig. 1(c)) and corresponds to the PSF along a specified direction ($\mathrm{LSF}(x) \approx \mathrm{PSF}(x)$) [9].

To model a two-dimensional, symmetric PSF, parameters of different statistical distribution functions are fitted to the one-dimensional $\mathrm{LSF}(x)$. The most common approach is the Generalized Gaussian (GG) distribution. The corresponding PSF is defined as

$$\mathrm{PSF}_{\mathrm{GG}}(x) = A \exp\left[-\left(\frac{x-x_0}{\alpha}\right)^{\beta}\right]. \tag{1}$$

Here, x denotes the distance along the slanted-edge region, A the amplitude, x_0 the center of the distribution, α a scaling parameter, and β a shape parameter. Note that the GG reproduces the standard Gaussian with $\beta = 2$ [4]. Another widely used model, particularly in astronomical PSF reconstruction, is the Moffat function. Its PSF model is calculated as

$$\mathrm{PSF}_{\mathrm{Moffat}}(x) = A\left[1+\left(\frac{x-x_0}{\alpha}\right)^2\right]^{-\beta}, \tag{2}$$

where the parameters have analogous meanings as in Eq. 1 [10]. Additionally, a weighted combination of the GG and Moffat functions, termed Generalized Pseudo-Voigt (GPV), is applied to combine their complementary characteristics [11]. This provides greater flexibility to reproduce both the central peak and broader tails of the experimentally determined LSF than either model individually. The weighting parameter η controls the relative influence of the GG and Moffat components. Exemplary reconstructed PSFs are shown in Fig. 1(d) and were subsequently used for image deconvolution with MATLAB's RL algorithm [5], [6]. To prevent artifacts (overshoots in the line profile) arising from modifications in the frequency response, each iteration step is additionally damped using a damping parameter ξ.

II.II. Metrics for image quality

To evaluate the deconvolution results, a duplex wire image quality indicator (IQI) was used (see Fig. 1(a)). It was recorded with the VAREX detector XRD 4343N-F45-N-060 with a pixel size of 150 µm. The IQI consists of a series of wire element pairs made from high-density metals (e.g. platinum and tungsten). The diameter of the duplex wires, which equals their wire spacing distance, decreases continuously. The exact design of the device is specified in the ASTM E2002 standard [8]. The modulation depth for each wire pair is determined from the contrast between the dips A, B, and C (cf. inset of Fig. 1(e)), which are obtained from the averaged line profiles of the duplex wire IQI (cf. blue rectangle in Fig. 1(a)). The resulting contrast K is defined as $K = (A+B-2C)/(A+B)$ [8]. The interpolated basic spatial resolution ($\mathrm{iSR_b}$) is determined where $K(\mathrm{iSR_b}) = 20\%$, obtained by non-linear regression of the contrast data according to

$$K(x) = p_0 - p_1 \exp(-p_2 x). \tag{3}$$

Here, x is the distance along the duplex wire IQI and p_0, p_1 and p_2 are the fit parameters (see orange line in Fig. 1(f)) [8], [12]. To characterize the artifacts of the deconvolution, a metric for the artifact error Δ was defined as $\Delta = \frac{O}{P}100\%$. As shown in Fig. 1(g), O is the relative overshoot height and P is the maximum-peak amplitude.

III. Results and discussion

First, the results of the iterative RL deconvolution using the four presented PSF models were evaluated without further damping, i.e., $\xi = 0$ (compare Sec. II.I). Figure 2(a) shows the $\mathrm{iSR_b}$ values and artifact errors achieved with the four different PSF models. The overall curve shape of the $\mathrm{iSR_b}$ functions is similar to that of a decreasing sigmoid function. The data points for the various models cease to exist at different numbers of iterations because the algorithm terminates prematurely once excessive artifacts occur.

The input image has an $\mathrm{iSR_b}$ of 192 µm and shows no artifacts ($\Delta = 0\%$). The best $\mathrm{iSR_b}$ improvement of 17% was observed with the GPV PSF model, resulting in an $\mathrm{iSR_b}$ of 159 µm (see purple curve in Fig. 2(a)). The artifact error Δ increases with the number of iterations for all PSF models, following a trend opposite to the $\mathrm{iSR_b}$ improvement. Since the GPV PSF provided the best compromise between resolution improvement and artifact formation within the investigated models, it was selected for the subsequent damping-parameter analysis.

To study the influence of the damping parameter of the RL algorithm, the GPV PSF model is used under variation of ξ. It is recommended to set ξ approximately equal to the standard deviation of the input image. Figure 2(b) shows the $\mathrm{iSR_b}$ and artifact error Δ versus the

10.18416/SCP.2026.2583
© 2026 Infinite Science Publishing

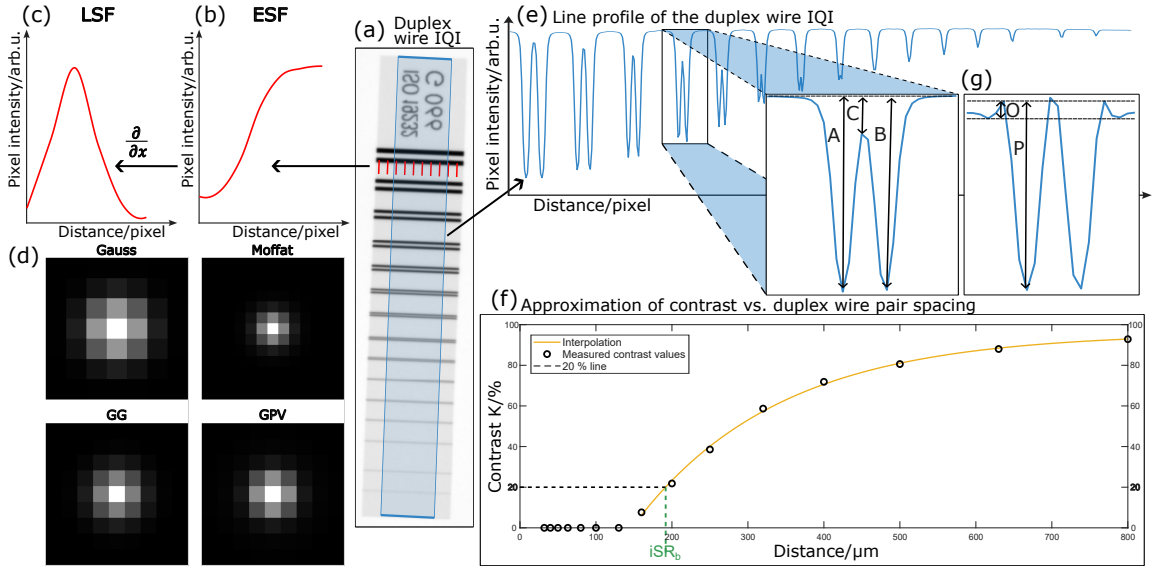


Figure 1: Methodology for PSF extraction (left) and resolution measurement (right). (a) Input image of a duplex wire IQI acquired with a 2–5° inclination according to [8]. Ten line profiles (red) were averaged to obtain the ESF (b), which was differentiated to obtain the LSF (c). The LSF was fitted using Gaussian, GG, Moffat, and GPV functions. All PSFs are energy-normalized (d). The deconvolution performance was quantified using the iSR_b from 20 averaged line profiles (blue rectangle). The wire-pair contrasts were calculated from the peak heights A, B, and C (e) and fitted according to Eq. (3) (f). The intersection at 20% contrast defines the iSR_b; the artifact error is determined from the overshoot-peak ratio (g).

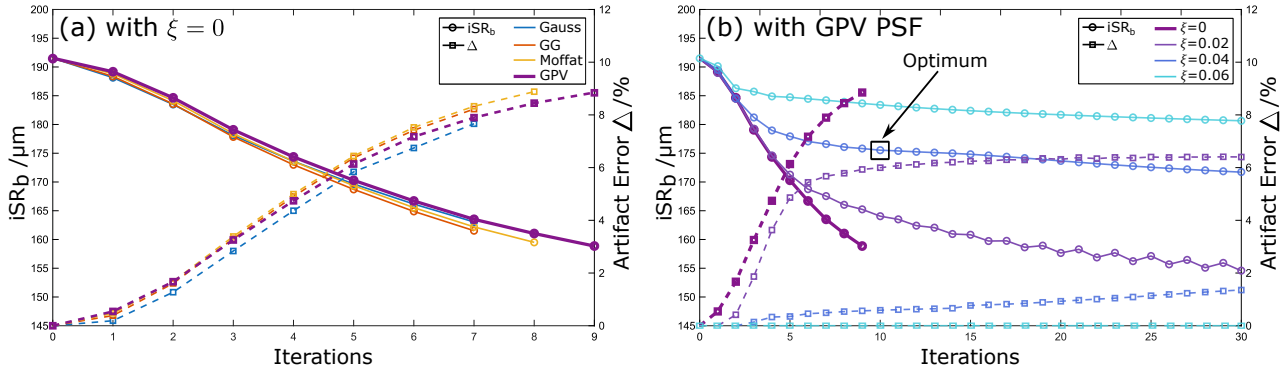


Figure 2: Values of the iSR_b and artifact error Δ versus the number of RL iterations for different PSF models without damping ($\xi = 0$) (a) and for a GPV PSF for different damping parameters ξ around the measured standard deviation of the studied input image (b). Within the investigated parameter range, $\xi = 0.04$ with ten iterations was identified as the best compromise between resolution enhancement and artifact formation.

number of iterations for the GPV PSF model (violet line in (a)) for a variation of ξ around the measured standard deviation of $\sigma = 0.022\,\mu m$ for the studied input image, derived from the overall intensity variance. It is discernible that an increase in the damping parameter ξ leads to slower convergence, necessitating more iterations for resolution enhancement. For $\xi = 0$ and 0.02, a large decrease in iSR_b but also a large increase in the artifact error Δ is realized. In contrast, for $\xi = 0.06$, the artifact error Δ remains quite small but nearly no iSR_b improvement is recognized.

Thus, within the investigated parameter range, $\xi = 0.04$ and ten iterations were identified as the best compromise between resolution improvement and artifact formation. The parameter selection was empirical and based on a limited set of damping parameters and iteration numbers.

The deconvolved image with these selected parameters (ten iterations and $\xi = 0.04$) is shown in Fig. 3(b). In comparison to the input image, a significant improvement in spatial resolution is visible. Particularly, in the zoomed-in areas of the 5th and 6th duplex wire pairs, the contrast between high-density metal and background increased significantly (see dotted orange and solid blue curves in the right inset of Fig. 3(b)).

Since the optimization was performed for only a few

10.18416/SCP.2026.2583
© 2026 Infinite Science Publishing

IQIs and imaging configurations, the transferability of the obtained parameters to other objects and acquisition conditions remains to be investigated. A systematic optimization including a more sensitive artifact metric could further improve the parameter selection, particularly for subtle artifacts.

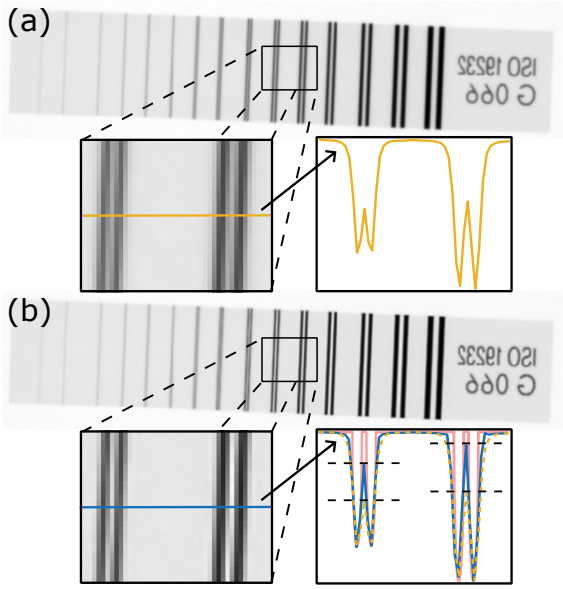


Figure 3: Illustration of resolution improvement by comparing the input image (a) with the deconvolved image (b) obtained using the selected parameters from Fig. 2(b). Both show a zoom-in on the 5th and 6th duplex wire pairs and the corresponding intensity profiles (yellow and blue, respectively, together with the ideal intensity profile in rose).

IV. Conclusion

This study demonstrated retrospective spatial-resolution enhancement of X-ray images using Richardson-Lucy (RL) deconvolution and slanted-edge-derived PSFs. Among the investigated models, the Generalized Pseudo-Voigt (GPV) PSF provided the best compromise between iSR_b improvement and artifact formation. Without damping, the GPV PSF yielded a maximum iSR_b improvement of 17%. Using the selected damping and iteration parameters, an improvement of over 9% was achieved with limited artifact formation.

However, the optimization was limited to only a few IQIs and imaging configurations, so the transferability of the obtained parameters to other objects and acquisition conditions remains unverified. Future work will address systematic parameter optimization, improved artifact quantification, and validation using different objects and acquisition conditions. The potential impact of the improved 2D image resolution on three-dimensional reconstruction will also be investigated.

Acknowledgments

The work has been carried out at VisiConsult X-ray Systems & Solutions GmbH, Stockelsdorf and supervised by the Institute of Medical Engineering, Universität zu Lübeck.

Author's statement

Conflict of interest: Authors state no conflict of interest. AI was used for linguistic fine-tuning.

References

[1] S. Zabler, A. Klos, P. Lhuissier, L. Salvo, M. Farahmandi, and S. Wittl. Denoising and deconvolving ct images of unknown origin: Comparing linear Wiener-deconvolution with deep convolutional neural network noise2inverse. *e-Journal of Nondestructive Testing*, 30(2), 2025, doi:10.58286/30718.

[2] U. Zscherpel, K. Osterloh, U. Ewert, and B. Berlin. Unsharpness characteristics of digital detectors for industrial radiographic imaging. *Journal of Nondestructive Testing*, 9, 2004. URL: https://www.ndt.net/article/dgzfp03/papers/v22/v22.htm.

[3] S. K. Dwivedi, M. Vishwakarma, and P. Soni. Advances and researches on non destructive testing: A review. *Materials Today: Proceedings*, 5(2):3690–3698, 2018, 7th International Conference of Materials Processing and Characterization, March 17-19, 2017. doi:10.1016/j.matpr.2017.11.620.

[4] M. S. Hosseini and K. N. Plataniotis. Convolutional deblurring for natural imaging. *IEEE Transactions on Image Processing*, 29:250–264, 2020, doi:10.1109/tip.2019.2929865.

[5] W. H. Richardson. Bayesian-based iterative method of image restoration. *Journal of the Optical Society of America*, 62(1):55, 1972, doi:10.1364/josa.62.000055.

[6] L. B. Lucy. An iterative technique for the rectification of observed distributions. *The Astronomical Journal*, 79:745, 1974, doi:10.1086/111605.

[7] N. Dey, L. Blanc-Feraud, C. Zimmer, P. Roux, Z. Kam, J.-C. Olivo-Marin, and J. Zerubia. Richardson–lucy algorithm with total variation regularization for 3d confocal microscope deconvolution. *Microscopy Research and Technique*, 69(4):260–266, 2006, doi:10.1002/jemt.20294.

[8] ASTM E2002, Standard practice for determining total image unsharpness and basic spatial resolution in radiography and radioscopy, ASTM, 2015.

[9] J. Yu, Y. Zhang, B. Qi, X. Bai, W. Wu, and H. Liu. Analysis of the slanted-edge measurement method for the modulation transfer function of remote sensing cameras. *Applied Sciences*, 13(24):13191, 2023, doi:10.3390/app132413191.

[10] M. Schuckman, R. Prouty, D. Chapman, and D. Engel, Using Moffat profiles to register astronomical images, in *Computer Vision – ECCV 2022 Workshops*, L. Karlinsky, T. Michaeli, and K. Nishino, Eds. Cham: Springer Nature Switzerland, 2023, 80–95, ISBN: 978-3-031-25056-9. doi:10.1007/978-3-031-25056-9_6.

[11] T. Ida, M. Ando, and H. Toraya. Extended pseudo-Voigt function for approximating the Voigt profile. *Journal of Applied Crystallography*, 33(6):1311–1316, 2000, doi:10.1107/s0021889800010219.

[12] S. Kramer, Entwicklung einer normgerechten Detektor-Evaluation für die zerstörungsfreie Röntgenprüfung im Kontext Industrie 4.0, Bachelorthesis, Technische Hochschule Lübeck, 2025.

© 2026 Infinite Science Publishing